Melo-Fonseca, F.; Lima, R.; Costa, M. M.; Bartolomeu, F.; Alves, N.; Miranda, A.; Gasik, M.; Silva, F. S.; Silva, N. A.; Miranda, G.

45S5 BAG-Ti6Al4V structures

Published in:
Materials & Design

DOI:
10.1016/j.matdes.2018.08.056

Published: 15/12/2018

Document Version
Publisher's PDF, also known as Version of record

Materials and Design 160 (2018) 95–105

Contents lists available at ScienceDirect

Materials and Design

journal homepage: www.elsevier.com/locate/matdes

45S5 BAG-Ti6Al4V structures: The influence of the design on some of the physical and chemical interactions that drive cellular response

F. Melo-Fonseca [a,b,*], R. Lima [c,d], M.M. Costa [a], F. Bartolomeu [a], N. Alves [e], A. Miranda [c,d], M. Gasik [f], F.S. Silva [a], N.A. Silva [c,d], G. Miranda [a]

[a] Center for Micro-Electro Mechanical Systems (CMEMS-UMinho), University of Minho, Campus de Azurém, 4800-058 Guimarães, Portugal
[b] MIT Portugal Program, School of Engineering, University of Minho, Guimarães, Portugal
[c] Life and Health Sciences Research Institute (ICVS), School of Medicine, University of Minho, Campus de Gualtar, 4710-057 Braga, Portugal
[d] ICVS/3B's - PT Government Associate Laboratory, Braga/Guimarães, Portugal
[e] Centre for Rapid and Sustainable Product Development (CDRSP), Polytechnic Institute of Leiria, Rua General Norton de Matos, Apartado 4133, 2411-901 Leiria, Portugal
[f] Department of Chemical and Metallurgical Engineering, School of Chemical Engineering, Aalto University Foundation, 00076 Aalto, Espoo, Finland

HIGHLIGHTS

- Ti6Al4V cellular structures were produced by additive manufacturing and bioactive glass impregnated by press and sintering
- This design promotes bone ingrowth into the structure as the bioactive is absorbed and replaced by newly formed bone
- The bioactive glass quantity on these structures had influenced the medium pH, greatly influencing the cellular viability
- The influence of these structures design on physical/chemical aspects was determined and biologically validated in vitro

GRAPHICAL ABSTRACT

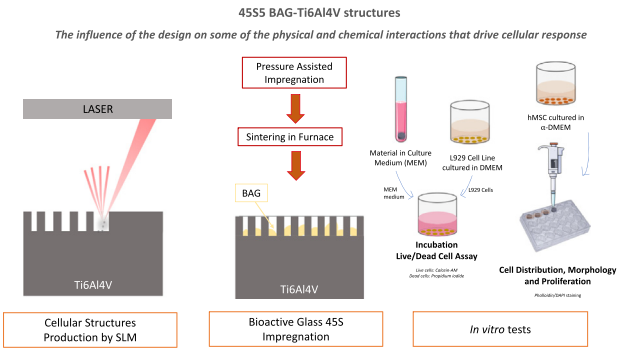

ARTICLE INFO

Article history:
Received 14 June 2018
Received in revised form 2 August 2018
Accepted 28 August 2018
Available online 30 August 2018

Keywords:
Multi-material cellular structures
Selective Laser Melting
Press and Sintering
Ti6Al4V
Bioactive glass 45S5

ABSTRACT

Multi-material Ti6Al4V cellular structures impregnated with 45S5 bioactive glass were designed and produced using Selective Laser Melting (SLM), an additive manufacturing technique, combined with Press and Sintering focusing on load bearing components like hip implants. These structures were designed to combine Ti6Al4V mechanical properties and promote bone ingrowth into the structure as the bioactive material (45S5) is being absorbed and replaced by newly formed bone.
The influence of these structures design on some of the physical and chemical aspects that drive cellular response was assessed. Roughness, wettability, bioactive glass quantity and quality on the structures after processing and the pH measured during cell culture (as a consequence of bioactive glass dissolution) were evaluated and correlated with cellular viability, cellular distribution, morphology and proliferation on the surface and inside the structures.

1. Introduction

Multi-material design is a trending approach for hip implants since it allows the gathering of distinct properties of dissimilar materials,

* Corresponding author at: Center for Micro-Electro Mechanical Systems (CMEMS-UMinho), University of Minho, Campus de Azurém, 4800-058 Guimarães, Portugal.
E-mail address: francisca.rmfonseca@hotmail.com (F. Melo-Fonseca).

https://doi.org/10.1016/j.matdes.2018.08.056

unachievable by mono-material solutions. The multi-functionality of Ti6Al4V structures impregnated with 45S5 Bioglass (BAG) is guaranteed once Ti6Al4V assures the mechanical stability of the implant and the incorporation and further replacement of BAG for newly formed bone promotes the fixation of the implant and bone ingrowth.

Aseptic loosening is still the major cause of revision surgeries in orthopedic implants, namely those used in total hip arthroplasty [1–3]. This loss of fixation is due to wear debris and mostly to stress shielding that is a consequence of the mismatch between the Young's moduli of the implant and bone [2,4–7].

Despite the use of metallic materials with lower Young's moduli, for example Ti6Al4V, the mismatch between implant and bone is still about 550% (ratio 5.5:1). Ti6Al4V is frequently used in orthopedic and dental implants since it possesses high biocompatibility and excellent corrosion resistance due to the formation of an oxide layer [2,8]. However, its bioinertness may result in lower osteointegration [9]. Porous structures made of titanium alloys not only mimic the mechanical properties of bone to minimize stress shielding, but also enhance bone ingrowth by promoting implant fixation, vascularization and flow of nutrients and waste [8,10,11]. There is no consensus about the optimum pore size in open cells to promote bone ingrowth and vascularization. Whereas some authors have stated that the pore size should be between 100 and 400 μm [12,13], others concluded that it should be around 600 μm [14].

A current trend regarding materials development for implants is their surface modification to modulate the cell behavior and promote tissue regeneration and also to act as antibacterial agents [15,16]. Recent works show the potential of Ti6Al4V composite coatings made of AgNPs (Ag nanoparticles) and HA, combined with additional compounds, to provide bacterial resistance and improved osteogenesis, due to the long-term release of Ag^{+}, as well as rapid osteointegration [17,18]. Similar outcomes regarding antibacterial activity, minimized cytotoxicity effects and osteoinductivity enhancement were also found when biofunctionalizing ZnO/polydopamine/arginine-glycine-aspartic acid-crysteine nanorod on Ti [19] and also when strontium and zinc oxides are doped into titania nanotubes in Ti-based materials [20]. These coatings can also incorporate drugs, as shown by a study where SLM-fabricated Ti6Al4V is surface functionalized with phosphonic acid monolayers with Paracetamol [21]. Even in structures this strategy is being used, creating coatings inside these structured components. CpTi-collagen and TiTa-collagen biphasic scaffolds have been developed for tissue engineering, using selective laser melting and type I collagen infiltration [22] to provide bone-like mechanical properties, while having the potential to support cartilage growth.

To improve fixation of implants, bioactive materials, including 45S5 Bioglass (chemical composition of 45 wt% is SiO_2, 24.5 wt% Na_2O, 24.5 wt% CaO and 6 wt% P_2O_5 [23–25]) are intended to interact with the biological environment [26]. Once bioglasses are similar to the natural apatites of bone and are reactive materials, they are able to bind to the surrounding bone tissue and promote osteointegration [27]. In more detail, these bioactive materials react with biological fluids and form a biologically active carbonated hydroxycarbonate apatite layer [28–30]. This layer, in turn, allows the attachment, proliferation and differentiation of osteoprogenitor cells that will consequently lead to calcium phosphates and collagen mineralization on the material's surface [25,30]. Despite these osteogenic properties, 45S5 bioglass sintering process has to be particularly cautious, once 45S5 crystallization occurs at temperatures between 550 °C and 610 °C but fully densification is achieved at 1000 °C [24,28,31]. Moreover, bioactive glasses are brittle which limit their use to non-loading applications [32].

To expand the use of BAG to load-bearing applications and improve osteointegration of metallic implants, coatings of bioactive glass on metals are usually performed. These coatings not only enhance the kinetics of bone formation but also the stability of the materials [14,33]. Despite the improvement of bone bonding and consequent osteointegration, bond sites between coating and implant have irregular geometries that can act as stress concentrations, referred as notch effects [5]. Another undesired outcome raised from implantation of coated materials is the detachment of the bioactive layer because of the strength required to place the implant in the human body [34]. Drnovšek et al. studied the effect of a porous titanium layer on Ti6Al4V implant, impregnated with bioactive glass powder, on osteointegration *in vivo*. Within ten weeks of implantation, the bioactive glass was completely resorbed and substituted with well attached newly formed bone, which overgrew the entire thickness of the porous structure [32]. Besides the bioactive properties, incorporation of BAG increases the macro-hardness of the multi-material design, and thus the wear resistance. This result was stated previously, where nanostructures of Ti-45S5 BAG composites showed an increase of Vickers Hardness compared to the pure microcrystalline Ti metal [35].

The attempt to replicate the host bone in orthopedic implants is hard, since bone composition and properties are specific for each person. The need for customization presents some complexity, namely concerning the design and manufacture of bone scaffolds [8]. Compared with conventional methods like casting, machining and hot forging, powder metallurgy is able to produce constructs with higher precision and better surface finishing [36–38]. Metal additive manufacturing (AM) or mostly known metal 3D printing, include some powder based technologies like powder bed fusion (PBF) technology [39,40]. These new techniques allow the fabrication of customized 3D scaffolds with controlled geometric shapes, since it can be coupled with computer aided design (CAD) model based on computed tomography or magnetic resonance imaging 3D data [8,10,41]. Besides the design freedom, this technology reduces considerably the amount of waste material and use of resources, produces with faster rates and uses less energy intensiveness [40,42,43].

Selective Laser Melting (SLM) is a PBF technique which has been used to produce 3D titanium-based materials targeting biomedical applications by fabricating components in a cyclic process [44–46]. The components are fabricated layer-by-layer using a laser source to melt powder beds [47]. As a layer-wise technique, SLM versatility allows the production of customized products with complex geometries such as titanium cellular structures [48,49].

Although the rapid heating-cooling cycles of laser scan, higher laser powers are related with more thermal energy accumulated at the top surface which, in turn, results in higher temperature gradient when producing Ti6Al4V parts by SLM [50]. In this sense, bioceramic parts cannot be produced by Direct AM techniques, once bioactivity is limited when using higher sintering temperatures [51,52]. Furthermore, the absence of commercial equipments available to fabricate metallic and bioceramics multi-materials and the difficulty of the process strategy justify the combination of two fabrication techniques.

In the present study, multi-materials structures of Ti6Al4V were produced by SLM followed by impregnation of 45S5 BAG, for load bearing applications, like hip replacements. The constructs design was physically validated by surface characterization techniques and biologically validated by cell cytotoxicity and proliferation assessments.

2. Materials and methods

2.1. Cellular structures production

A 6 mm diameter rod of Ti6Al4V alloy was purchased from Titanium Products (United Kingdom). The titanium rod was cut in order to obtain discs with, approximately, 3 mm in height. Then, the discs were sandblasted for 30 s using spherical alumina particles with a granulometric range between 106 and 150 μm. These commercial samples were subjected to a surface treatment to achieve a moderately rough sandblasted and acid-etched (SLA) surface (2–4 μm (Ra)), which are the material conditions commonly used in today's hip implants [53,54]. After sandblasted, the samples were acid etched with the following solution: 32% HCL, 96% H_2O_4 and H_2O (2,1,1). The acid

etching was performed at 65 ± 3 °C for 5 min, followed by isopropanol cleaning, also during 5 min. This group of samples was categorized as S1.

Cellular structures made of Ti6Al4V (SLM Solutions GmbH, Germany), were produced by SLM (SLM Solutions, model 125 HL), and named S2. The fabrication parameters of the laser were 90 W, scan speed of 600 mm/s, spacing of 70 μm, and a layer thickness of 30 μm. These parameters were based in previous studies that already described the optimum processing parameters for Ti6Al4V structures [55,56]. Metallic scaffolds were printed with a pore size of 450 μm and a wall thickness of 300 μm, and the pores are interconnected in all directions (vertically and horizontally), as can be seen in the schematic representation of Table 1.

After printing the cellular structures, these were impregnated with two different weight percentages of BAG, purchased from mosci Corporation, thus obtaining two types of samples: S3 and S4. Each one of these impregnated samples (S3 and S4) was weighted before and after the impregnation process. The ratio between the mass of bioactive (difference between the sample weight after and before the impregnation) and the final weight of the sample (with bioactive) was calculated and named "bioactive percentage".

The first set of samples (group S3) was positioned inside an ultrasonic equipment and immersed in a BAG powder and acetone solution 15% (w/v). After being heated, until evaporation of acetone, they were sintered in a tubular furnace at 600 °C for 2 h, under high vacuum, with a heating and cooling rate of 5 °C/min. The bioactive percentage of S3 group was of 2.05 wt%.

The second impregnation method was comprised of a Press and Sintering technique. The cellular structures were placed inside a steel mold and then immersed in a viscous solution of BAG powder and acetone 83% (w/v). Hydraulic pressure was applied for 10 min in order to impregnate all open cells and then sintering was performed. The specimens were sintered in a tubular furnace at 600 °C for 2 h, under high vacuum, with a heating and cooling rate of 5 °C/min. This last group of samples was denominated S4, where the bioactive percentage was equal to 2.50 wt%.

In addition to the "bioactive percentage", an "impregnation ratio" was calculated by dividing the weighted mass of bioactive inside the structures by the mass of bioactive that would totally fill the pores of the structures. In this sense, the impregnation ratio on impregnated samples was 37.34 and 47.29%, for S3 and S4, respectively.

Finally, all the produced samples, displayed in Table 1, were polished, until achieving similar surface conditions, with abrasive silicon carbide papers starting with P120 up to P4000. After polishing, they were ultrasonically cleaned during 10 min using isopropanol.

2.2. Scaffolds characterization

X-ray diffraction (XRD) analysis were performed for the commercial Ti6Al4V (S1), Ti6Al4V-based cellular structures fabricated by SLM (S2) and Ti6Al4V cellular structures impregnated with BAG (S3 and S4), using Bruker AXS D8 Discover equipment, with a 2Θ from 10 to 80° with a step size of 0.02 at 1 s per step. These XRDs allowed to assess the condition of BAG on the impregnated samples, after being sintered at 500 °C, 550 °C and 600 °C.

The produced scaffolds, unreinforced and BAG-impregnated, were analyzed using Scanning Electron Microscopy (SEM) using NanoSEM - FEI Nova 200 (FEG/SEM) equipment.

2.3. Surface roughness

The roughness was measured five times in each specimen using a contact profilometer (Surftest SJ 201, Mitutoyo, Tokyo, Japan) using $\lambda_c = 0.8$ μm, $\lambda_s = 2.5$ μm, and 0.25 mm/s. The parameters were selected according to the International Organization for Standardization number 4287, from 1997 [57]. For the scaffolds, the profilometer ran the samples along the metallic walls. The measured surface roughness parameters were the average roughness (Ra), the peak-to-valley roughness (Rz) and the root-mean-square roughness of the departures of the profile from the mean line (Rq).

2.4. Wettability

Contact angle measurement was used to determine wettability properties of the metallic scaffolds, by the sessile drop technique using the contact angle system OCA 15 plus (Dataphysics). Five droplets of water or phosphate-buffered saline (PBS) were measured for each group sample and the average was taken for each result.

2.5. Cytotoxicity assessment

The short-term cytotoxicity of the produced scaffolds was performed as previously described [58–61], in triplicate. The scaffolds were placed in minimum essential medium (MEM) and extracted after 24 h, 7, 14, 21 and 28 days. In all tests, material weight-to-extract fluid rate was constant (0.2 g/mL) and after each time point the extracts were filtered through a 0.45 mm pore-size filter.

2.5.1. Cell culture

Rat lung fibroblasts-L929 cell line from European Collection of Cell Cultures were seeded in a 24-well plate ($n = 3$, 5×10^3 cells/well) and then cultured at 37 °C in a humidified atmosphere with 5% CO_2, for 24 h in Dulbecco's modified Eagle's medium (DMEM) culture medium (Dulbecco's modified Eagle's medium) (Sigma). This media was supplemented with 10% fetal bovine serum (FBS) (Gibco, Barcelona, Spain) and 1% antibiotic-antimycotic mixture (Sigma).

2.5.2. MEM extraction test

Twenty-four hours after cell seeding, the culture medium was removed from the wells and replaced by the MEM extraction fluid. The L929 cultures were then incubated for 72 h at 37 °C in a humidified atmosphere with 5% CO_2. Live cells were stained with calcein-AM (1 mg/mL; Molecular Probes, Eugene, OR) and nonviable cells with propidium iodide (0.1 mg/mL; Molecular Probes). After incubation for 15 min at 37 °C in a humidified atmosphere with 5% CO_2, cultures were observed under a fluorescence microscope, with an excitation

Table 1
Groups detailed description.

Representation	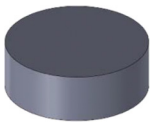			
Group number	S1	S2	S3	S4
Description	Ti6Al4V CAST SLA treated	Ti6Al4V SLM	Ti6Al4V SLM impregnated with BAG (2.05 wt%)	Ti6Al4V SLM impregnated with BAG (2.50 wt%)

wavelength of 490 nm (BX-61; Olympus, Hamburg, Germany). Latex extracts were used as positive controls for cell death, whereas standard culture medium was used as negative control.

Besides images analysis, the effect of scaffolds leachables on the medium pH was assessed in each group medium by inoLab pH 720 (WTW, Germany).

2.6. Direct contact assay

Cell attachment and proliferation can be assessed by direct contact assay in order to evaluate the *in vitro* biocompatibility of the scaffolds. Human Mesenchymal Stem Cells (hMSCs) derived from human bone marrow (Lonza, Switzerland) were cultured as monolayers in Alpha minimum essential medium (α-MEM). This medium was supplemented with 10% FBS and 1% antibiotic-antimycotic mixture, in sterile T175 tissue culture flasks.

Cell seeding was performed as previously described [62]. Briefly, the P6 hMSCs were trypsinized, centrifuged and resuspended in α-MEM medium. Subsequently, 50 μL of medium containing 1×10^5 cells were seeded on top of the scaffold. One hour after cell seeding, 750 μL of culture medium was added to each well and cell-scaffold were incubated for 3 and 7 days in a humidified atmosphere at 37 °C, containing 5% CO_2, with medium changes every 3 days.

2.6.1. Cell distribution, morphology and proliferation

After 3 and 7 days of culture, the distribution and morphology of the hMSCs were evaluated using *phalloidin/DAPI* staining [63]. *Phalloidin* labells cytoskeleton (red) whereas the nucleus is stained with *DAPI* (4′,6-diamidino-2-phenylindole) (blue). After cells fixation with paraformaldehyde (PFA) 4% for 30 min at room temperature, the cell-scaffold structure was washed and sliced. Both the top and the sliced scaffold structures were incubated with 0.1 μg/mL of *phalloidin* (Sigma) and 1 μg/mL of *DAPI* (Sigma) during 30 min. Finally, scaffolds were washed with PBS and observed under a confocal microscope (Fluoview FV 1000; Olympus, Hamburg, Germany).

2.7. Statistical analysis

In order to investigate surface roughness differences between groups, one-way ANOVA with *post hoc* Bonferroni's multiple comparison test was performed.

Wettability differences between groups and between both solutions (water and PBS) were assessed by performing a two-way ANOVA with *post hoc* Bonferroni's multiple comparison test.

In order to investigate cytotoxicity differences between groups for each timepoint, the non-parametric Mann–Whitney test was performed.

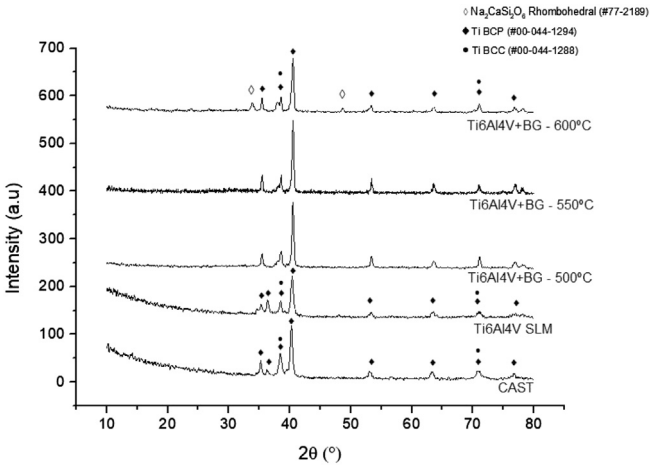

Fig. 2. X-ray diffraction pattern of commercial sample Ti6Al4V (S1), SLM processed Ti6Al4V structures (S2), and SLM processed Ti6Al4V structures impregnated with 45S5 BAG (S3) sintered at different temperatures.

Statistical significance was defined for $p < 0.05$ and GraphPad Prism v6 from GraphPad Software, California, USA was used for all the statistical analysis performed.

3. Results and discussion

3.1. Scaffolds characterization

Top surfaces of samples from each group (S1-S4) were analyzed by SEM (Fig. 1). S1 group represents the commercial solution used in hip implants and presents a sandblasted and acid-etched (SLA) topography. SLM as-fabricated samples (S2) micrograph (Fig. 1) shows the produced structure made from the CAD file. Moreover, these parts have high density since no significant surface porosity is detected. SEM images of the impregnated samples (S3 and S4) show that higher impregnation ratio is correlated with less free space inside the holes. Moreover, the impregnation process assures the mechanical interlocking between both materials, preventing the bioceramic's detachment.

Fig. 2 shows the X-ray diffractograms of the commercial Ti6Al4V, Ti6Al4V cellular structures fabricated by SLM and Ti6Al4V cellular structures impregnated with BAG, at different sintering temperatures. Ti6Al4V is a typical two phases $\alpha + \beta$ titanium alloy [64]. In Fig. 2 both phases are present in the commercial and SLM processed Ti6Al4V samples, being the main constituents of the SLM processing Ti6Al4V the martensitic phase. However, when processed by SLM, the phase β increased. This is due to the fast cooling rate of this additive manufacturing technique that does not allow the diffusion of V atoms

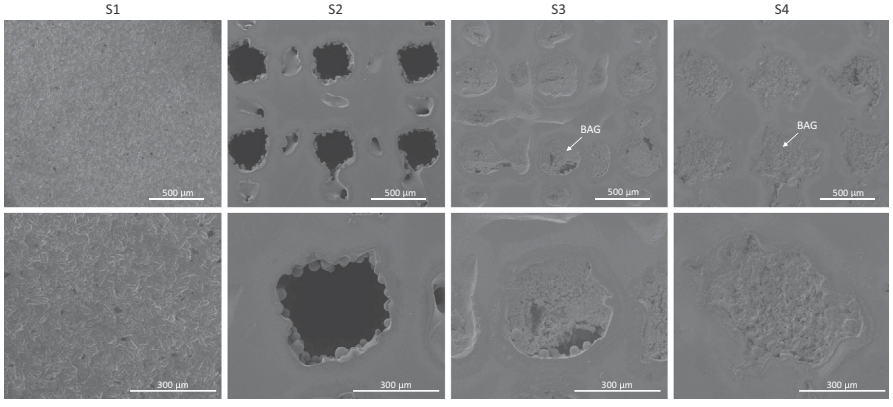

Fig. 1. SEM micrographs of commercial sample Ti6Al4V (S1), SLM processed Ti6Al4V structures (S2), and SLM processed Ti6Al4V structures impregnated with BAG, having a 2.05 wt% (S3) and 2.50 wt% (S4) of BAG.

Table 2
Roughness parameters measured on the four groups (mean ± SD).

Group name	Ra (μm)	Rz (μm)	Rq (μm)
S1	1.90 ± 0.10	14.17 ± 0.99	2.38 ± 0.09
S2	0.18 ± 0.04	2.13 ± 1.22	0.29 ± 0.13
S3	0.09 ± 0.01	1.14 ± 0.47	0.14 ± 0.03
S4	0.11 ± 0.03	1.49 ± 0.75	0.18 ± 0.08

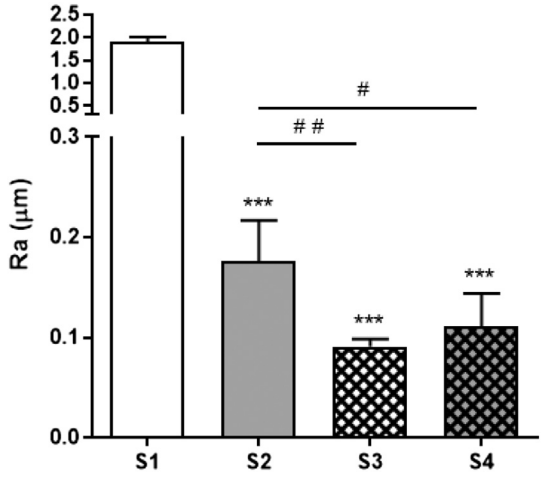

Fig. 3. Surface roughness values (Ra) for the four groups. Data are presented as mean ± SD (n = 5). Symbol *** denote statistically significant differences ($p < 0.001$) in comparison to S1, # and ## denote statistically significant differences ($p < 0.05$ and $p < 0.01$), respectively, comparative to S2.

in phase β and consequent transformation into phase α [65]. The Ti6Al4V cellular structures impregnated with BAG were analyzed by XRD, when sintered at four different sintering temperatures. Phase transformations of the glass powder may affect the sintering process due to nucleation and growth of crystalline phases [66].

Impregnated samples were found amorphous for sintering temperatures of 500 °C and 550 °C. In this study, the minimum temperature or achieving crystallinity was 600 °C. According to literature, crystallization of the bioglass corresponds to the first densification step and to the formation of $Na_2CaS_2O_6$, at 600 °C [66,67]. At 850 °C another densification takes place, being possible to identify a second crystalline phase, $Na_2Ca_4(PO_4)SiO_4$, at 1000 °C [66].

Once the increase of crystallinity slightly decreases the kinetics of the bioactive reaction and compromises the mechanical properties, no superior temperature to 600 °C should be used. Moreover, the precise control of Ti6Al4V samples impregnated with BAG by using vacuum atmosphere at 600 °C does not alter the microstructure of Ti6Al4V and maintains the mechanical properties of the initial components. In order to preserve the bioactivity and assure the best mechanical properties, the sintering temperature of 600 °C was chosen for further fabrication of impregnated samples.

3.2. Roughness

The surface properties of an implant are correlated with the cell behavior, since they affect the implant-cell interactions [68]. Among those properties, surface energy, which depends on surface charge, chemical composition and microstructural topography [69], appears to be a dominant factor concerning cell adhesion and proliferation [68]. Nonetheless, roughness can modulate the activity of cells, by changing the production of growth factors and cytokines by the cells [70].

The surface roughness values (Ra, Rz and Rq) acquired on the four groups are present on Table 2 and the statistical analysis of Ra in Fig. 3.

According to literature, commercial samples of Ti6Al4V pre-treated with SLA display a roughness (Ra) of 1.96 ± 0.07 μm, with the presence of etching-induced round-shaped grooves [71]. Taboreli et al. [72] have referred that one of the possible factors that explain why acid etching may increase Ra is the hydrogen desorption, which in turn results in an increase of the subsurface hydrogen concentration and the formation of titanium hydride (TiH_2).

Ti6Al4V samples produced by SLM displayed a Ra of 19.75 ± 1.50 μm before polishing and after polishing (S2) this value decreased to 0.18 ± 0.04 μm. The roughness values (Ra) measured by other authors before and after polishing were 17.6 ± 3.7 μm and 0.437 ± 0.045 μm, respectively [73]. Although small differences between our results and the ones found in literature, SLM process results in imperfections on the surface of Ti6Al4V constructs (Fig. 4). These imperfections will act as holes and, therefore, contribute to the roughness of the whole specimen. However, after impregnation, these imperfections will be filled with the bioactive material, decreasing, therefore, the roughness of the sample. As shown in Table 2, the lowest roughness value was found for S3 samples with lower impregnation ratio (37.34%), however no significant differences were found between the roughness of samples from groups S3 and S4.

Regarding roughness, according to the statistical test, the SLM-fabricated samples (S2, S3 and S4) are statistically different comparing to the commercial one (S1). Besides these differences, there are statistical differences between the impregnated samples (S3 and S4) when compared individually to the cellular structure without bioactive material (S2), validating the previous claim on the filling of these defects by the bioactive.

According to literature, S2, S3 and S4 present adequate topography since material's surface with Ra lower than 1 μm have been correlated with significant cell proliferation, independently of the wettability of the scaffold [68].

3.3. Wettability analysis

Wettability was assessed in order to investigate the influence of surface charge on cell adhesion. Besides water contact angles, which were measured in order to be compared with the literature ones, PBS was also used as a representative of a biological fluid. The contact angles were measured in the moment when the drop touched the surface of each scaffold and, according to [74], hydrophobicity corresponds to contact angles higher than 65°. The as produced Ti6Al4V SLM-fabricated constructs had

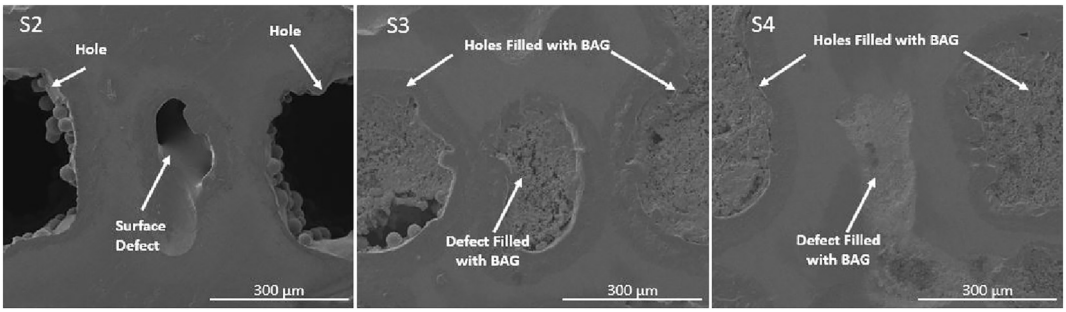

Fig. 4. SLM structures surface defects.

Table 3
Water and PBS contact angles (mean ± SD) of Ti6Al4V Cast, Ti6Al4V SLM structures, and Ti6Al4V structures impregnated with 2.05 wt% and 2.50 wt% BAG.

Sample group	Contact angle mean ± SD (°)	
	Water	PBS
S1	97.76 ± 3.02	92.90 ± 4.09
S2	Super hydrophilic	Super hydrophilic
S3	36.76 ± 3.01	19.30 ± 2.36
S4	38.56 ± 9.32	21.76 ± 3.49

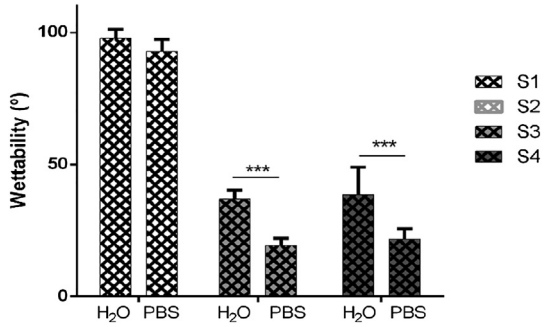

Fig. 5. Differences between water and PBS contact angles of S1, S3 and S4 groups. Data are presented as mean ± SD (n = 5). Symbol *** denotes statistically significant differences ($p < 0.001$) between both solutions.

a Ra of 19.75 ± 1.50 μm and water and PBS contact angles of 129.46 ± 5.0° and 120.78 ± 2.81°, respectively. Since hydrophilic surfaces are usually preferred rather than hydrophobic ones [75,76], all cellular structures (either impregnated or not) were polished. Both water and PBS contact angles of each scaffold group are present on Table 3, and the statistical analysis of Ti6Al4V Cast group (S1) and the impregnated groups (S3 and S4) between water and PBS contact angles are represented in Fig. 5.

Ti6Al4V cast (S1) is hydrophobic, and the difference between water and PBS contact angles is negligible. This value is close to that found on the study conducted by Chen et al. ($\Theta = 101°$) for the same material [71]. It was stated above that the hydrogen desorption leads to the formation of TiH_2 and in Chen et al. study, a contact angle of 153 ± 3° and roughness value at the nanoscale (3.29 ± 0.18 μm) was evaluated using atomic force microscopy [77]. In another study, the presence of hydrogen in the subsurface of a SLA commercially pure titanium [72] was considered accountable for this material hydrophobic behavior ($\Theta = 117 \pm 2.7°$).

Ti6Al4V SLM-fabricated (S2) is super hydrophilic since it was not possible to determine the static contact angle, as can be seen in Fig. 6. This super hydrophilicity is due, not only to the open cells, but also to the polished surface that allows the complete spreading of both water and PBS drops. Hydrophilic surfaces are usually preferred rather hydrophobic ones [76,75], since interaction between implant and tissues is enhanced. Both impregnated samples are hydrophilic with no statistically significant differences between groups (S3 *vs* S4), however each impregnated group shows statistically significant differences ($p < 0.001$) between water and PBS contact angles, being more hydrophilic when exposed to PBS (Fig. 5). Water contact angles reported in the literature of dense discs of 45S5 Bioglass are included in the hydrophilic range (14 ± 3° [78] and 14 ± 3° [79]). Since the impregnation of BAG fills the pores of the SLM-cellular structure, the lower impregnation ratio (37.34% for S3 as opposed to 47.29% for S4) results in more free spaces on the surface. Therefore, in spite of BAG hydrophilicity, the higher addition of BAG does not result in higher wettability because there are less free pores on the surface.

In fact, according to the Wenzel model [80], when in contact with rough structures, the liquid drop is fully into contact with the solid's surface. In the S1 group, for which the contact angle is higher than 90°, the SLA produced roughness enhances repellence, while for the polished groups (S2, S3 and S4) it enhances the liquid spreading [80]. Moreover, in porous structures, the water will pass through the pores if the pressure is sufficient to disrupt the surface film across the openings [80]. The model described by Cassie-Baxter [81] includes the air pockets which may be trapped between the gaps and thus, besides roughness, porosity affects the surface wettability.

The interconnected pores of SLM-fabricated specimens (S2, S3 and S4) increase the liquid-solid contact area, and therefore the capillary forces [82]. When the capillary forces overcome the pressure forces promoted by the air trapped inside the pores, the capillary-pressure balance is disrupted which eliminates the air pocket pressure effect. Consequently, the water and PBS drops spread inside the whole structure which increase the wettability of the surface.

The tendency found in all the groups tested, for an increased wettability (lower contact angles) when using PBS, as compared to water, can be due to the adsorbed solute ions such as Na^+ and Cl^-, that strongly influence the surface hydrophilicity and their ensuing osteoconductivity, as reported by some studies found in literature [83,84].

Until today it remains unclear what is the optimal degree of hydrophilicity for best biological and clinical outcomes [85]. However, moderate hydrophilicity is usually preferred, once cell adhesion decreases as the wettability is further decreased [86]. Hydrophilicity enhances the surface reactivity with the surrounding ions, amino acids and proteins, which promotes the bone cells attachment and proliferation and consequently osseointegration [87].

3.4. pH

Cells are surrounded by a microenvironment that can be affected by the degradation of the scaffold material [88]. Bioactive materials, as 45S5 Bioglass, when exposed to physiological solutions, start to biodegrade due to, among other processes, dissolution [89]. The dissolution of 45S5 Bioglass is accompanied by the release of Na^+, Ca^{2+}, Si products (presumably $Si(OH)_4$) into the external media [90]. This ion exchange with H^+ and H_3O^+ causes a rapid and last longing alkalization which, in turn, activates a regulatory phenomenon (in particular the Na^+/H^+ exchanger) that induces a shift in the internal pH to higher values [91]. Although the magnitude of change in the internal pH is smaller than that in the external pH, metabolism and functional effects in cells are observed [91]. Besides this phenomenon, the increase of pH has

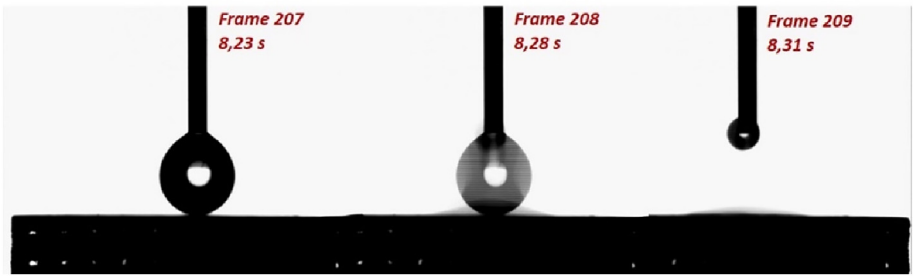

Fig. 6. Super hydrophilic behavior of Ti6Al4V SLM cellular structures (S2).

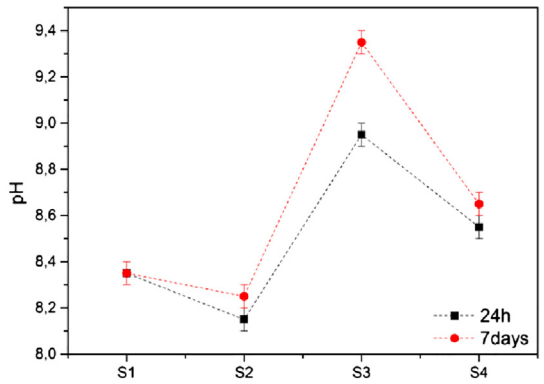

Fig. 7. pH variation of all groups at 24 h and after 7 days. Data are presented as mean ± SD.

been previously shown to confer antibacterial effects [92]. In addition, bioactive glasses also contribute to the remineralization [92].

Monfoulet et al. studied the effect BAG, HA/TCP and coral ceramics constructs when in contact with hMSCs for different alkaline pH [90]. All constructs presented similar physical properties (topography, roughness and available surface for cell attachment) but the pH measured in cell-containing BAG constructs was more alkaline than that detected for the two other materials. Although hMSCs viability and proliferation was not affected until pH 8.85, both *in vivo* and *in vitro*, the osteogenic differentiation was inhibited (particularly the expression of osteoblastic markers, namely alkaline phosphatase (ALP) activity and gene expression of RUNX2, ALP, and BSP), for pH values above 7.9. Moreover, for pH between 7.9 and 8.27, hMSCs proliferation was not affected but the osteogenic differentiation was substantially inhibited [90].

An optimal alkaline environment is beneficial for bone cells regarding the calcification, since at pH 7.35 collagen chains are crosslinked and consequently hyaluronic acid precipitates [93]. In another study, metabolic alkalosis (pH 7.6) decreased bone calcium efflux from bone by decreasing osteoclastic resorption and increasing osteoblastic formation [94]. In fact, voltage-activated calcium channels, located in osteoblasts membranes are inhibited by H^+ [95], which rises the intracellular calcium. 45S5 BAG was exposed to osteoblasts and fibroblasts, in order to infer its effect regarding pH changes [91]. An increase in intra- and extracellular pH and consequent $[Ca^{2+}]_i$ in osteoblasts slightly hyperpolarized the plasma membrane, increased the lactate production, and hence ATP generation by osteoblasts. Both in osteoblasts and fibroblasts, BAG did not enhance proliferation or increased ALP activity but metabolic effects were much smaller in fibroblasts than in osteoblasts [91].

In our constructs, when the physiological fluid enters through the open cells, it may be stagnated with the dissolution products. The effect of the scaffolds leachables was measured as a change in the medium pH, after culture of 24 h and 7 days (Fig. 7). Besides being the only group that presents a significant pH difference between both time points, S3 scaffolds contributed to the most alkaline medium. On the other hand, S2 has the lowest pH value. The lack of renewal of the medium inside the pores may increase the toxicity and this effect is highlighted for the lower impregnated samples (S3), compared to the higher impregnated ones (S4). Moreover, lower quantity of BAG is related with higher surface contact area with bioactive material which enhances the dissolution rate and consequently the pH of the medium.

3.5. Cell viability

The cytotoxicity assessment allows the analysis of toxic effect of the products released from the metallic scaffolds during the MEM extraction.

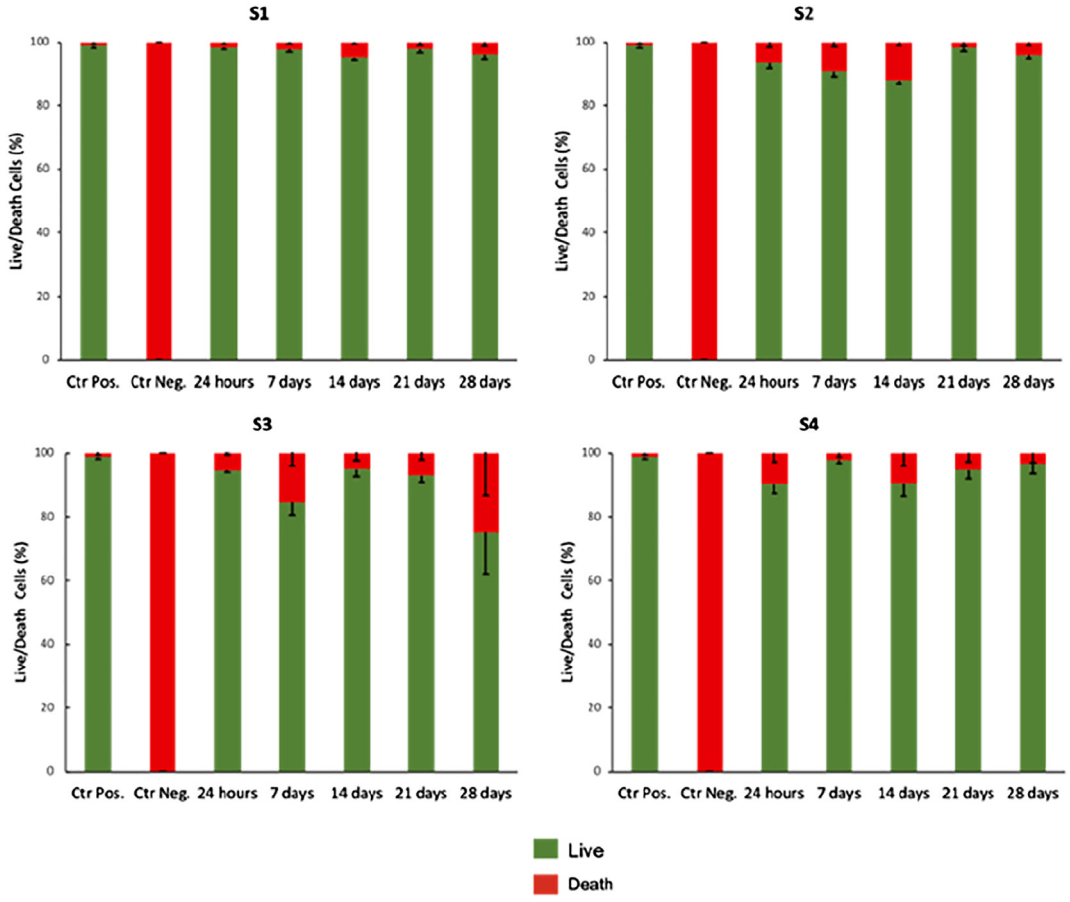

Fig. 8. Cell viability of L929 cells of the four groups, after an incubation with the extracts of 72 h.

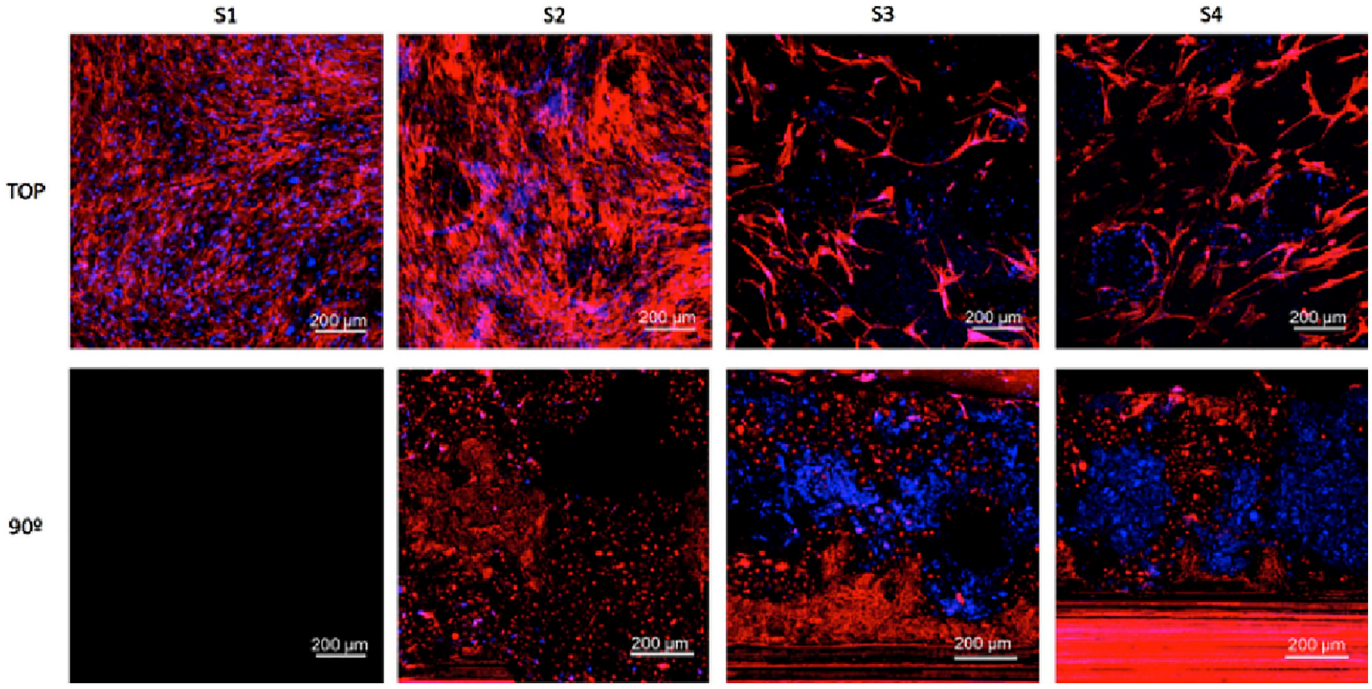

Fig. 9. Fluorescence microscopy images of hMSC cultured for 7 days on Ti6Al4V Cast (S1), Ti6Al4V SLM structures (S2), Ti6Al4V SLM structures with a 2.05 wt% of BAG (S3) and with a 2.50 wt% of BAG (S4). hMSCs were stained with *DAPI* (nucleus at blue) and with *phalloidin* (actin cytoskeleton at red). Images on the top are from the surface and, cross section images are on the bottom.

Fig. 8 shows the highest levels of viability in the Ti6Al4V Cast samples (S1), in every time points. The statistical analysis between the four groups was conducted (using the non-parametric Mann–Whitney test), and no statistically significant differences were found among groups, for each time point. Overall, we can assume that all four groups were not releasing significant toxic substances in the culture medium which encouraged cells proliferation and attachment. However, the leachables from group S3 seem to promote the higher toxic effects on L929 cells. This toxic effect on group 3 is sustained and seems to increase over time. This effect does not happen on the other groups, were at 28 days there no cytotoxic effect observed. This result makes the scaffolds from S3 the less suitable for cell culture.

The cell attachment is influenced, among other factors, by the surface energy. This, in turn, depends on surface chemical composition, surface charge and microstructural topography [75]. Regarding the surface charge, adhesion on metals increases linearly with surface hydrophilicity and materials with higher surface energy have higher cellular adhesion [69]. Fig. 9 represents the staining of the cells on the surface (top of Fig. 9) and also through the scaffold (bottom of Fig. 9). S1 group shows a densely and well distributed group of cells on the surface.

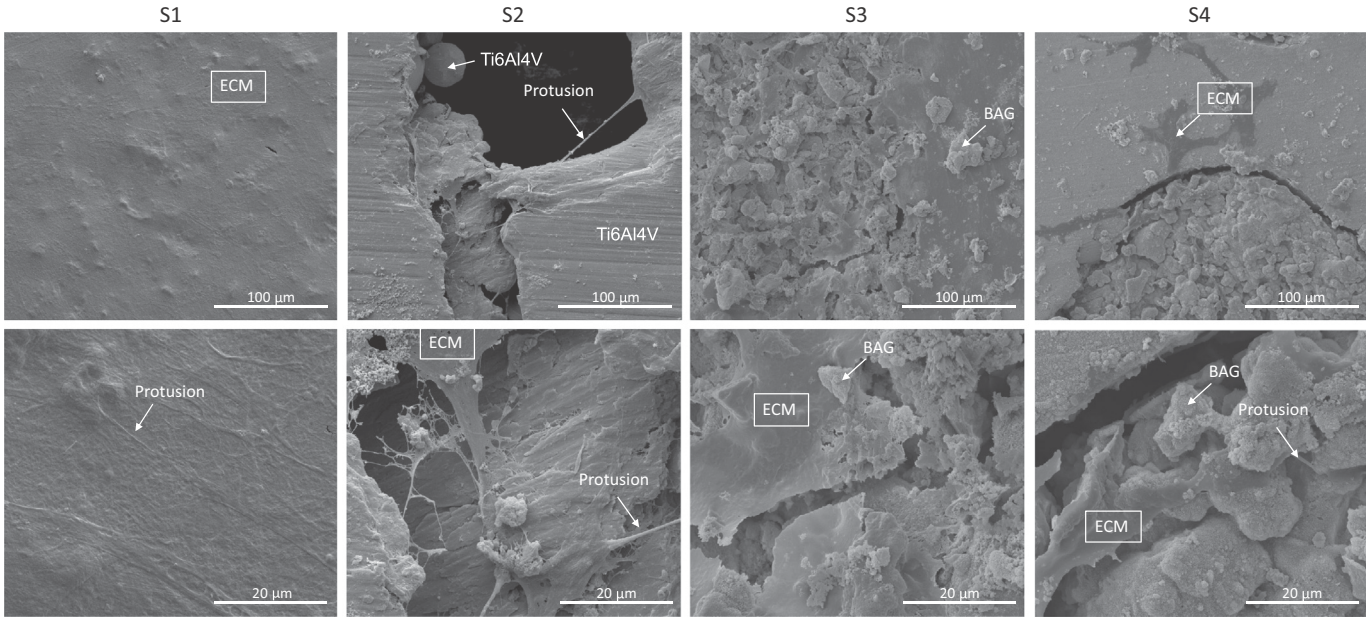

Fig. 10. Scanning electron micrograph of hMSC cultured on Ti6Al4V Cast (S1), Ti6Al4V SLM structures (S2), Ti6Al4V SLM structures impregnated with 2.05 wt% (S3) and 2.50 wt% (S4) of BAG, after an incubation of 7 days. Top images have a magnification of 1000 x and the bottom ones of 5000 x.

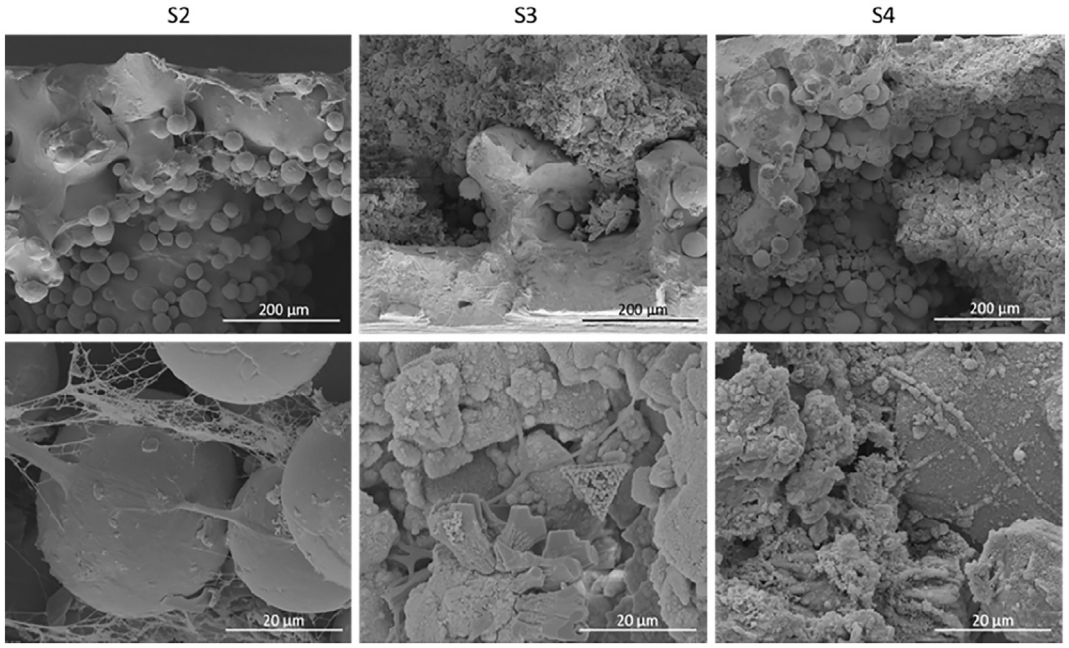

Fig. 11. SEM cross section micrographs of hMSC on Ti6Al4V SLM structures (S2), Ti6Al4V SLM structures with 2.05 wt% of BAG (S3) and with 2.50 wt% of BAG (S4), after an incubation of 7 days. Magnification of 500 x and 5000 x, on top and bottom images, respectively.

In the cellular structures without bioactive material (S2), actin cytoskeleton is stained around the pores but some cells are inside the pores, since they are also observed on the cross section images. Cells in S3 and S4 have a spindle-like shape and also triangular form, and are not so densely distributed. Comparing these last two groups, S4 shows an increase of the number of cells and *DAPI* stain is present on the BAG incorporation location.

Figs. 10 and 11 show the cell culture on each group sample. The Ti6Al4V Cast samples (S1) possess a moderately rough acid sandblasted and acid-etched (SLA) surface and, therefore, cells are well distributed. Cellular structures produced by SLM (S2) are rougher and cells protrusions are detected, which proves an adequate topography for cells culture. Regarding BAG impregnation, cells are flat and visible for both impregnation ratios. Taking into account the cross section images (Fig. 11), once again S2 shows cells protrusions, and thus the formation of extracellular matrix (ECM). Protrusions are not so detectable in S3 and S4 groups but, a carrier of cells is visible.

4. Conclusions

In the present study, Ti6Al4V cellular structures impregnated with 45S5 bioactive glass were designed and produced by using an Additive Manufacturing technique (SLM) combined with Press and Sintering. These multi-material structures present a novel multi-functionality approach for load bearing applications, like hip replacements, that assure no detachment of the bioactive material by using a mechanical interlocking between both materials. The impregnation process conducted on this study was validated, once the sintering temperature assured BAG's sintering while preserving its bioactivity.

The influence of the design on some of the physical and chemical interactions was assessed. The produced structures exhibited a hydrophilic behavior, once the interconnected pores of SLM-produced structures increase the liquid-solid contact area, which in turn, increase wettability. Regarding the impregnated samples, although no significant release of toxic substances to the culture medium occurred, the bioactive glass quantity on these structures had a direct influence on the medium pH which, in turn, had a great influence on the cellular viability. Based on the results of the cellular viability tests, higher impregnation ratios should be used on these structures in order to reduce the pH and obtain a moderate hydrophilicity and in this way assure an adequate environment for cell growth. Moreover, these structures can be useful drug carriers by adding anti-inflammatory, antibiotic, antimicrobial drugs to the bioactive materials.

Data availability

The raw/processed data required to reproduce these findings cannot be shared at this time due to time limitations and also to the fact that at this time this data also forms part of an ongoing study.

Acknowledgments

This work was supported by FCT (Fundação para a Ciência e Tecnologia) through the grants SFRH/BPD/112111/2015, SFRH/BD/128657/2017, PD/BDE/127836/2016, SFRH/BPD/97701/2013, SFRH/BD/141056/2018, SFRH/BD/140191/2018 and the projects PTDC/EMS-TEC/5422/2014 and NORTE-01-0145-FEDER-000018-HAMaBICo. Additionally, this work was supported by FCT with the reference project UID/EEA/04436/2013, by FEDER funds through the COMPETE 2020 – Programa Operacional Competitividade e Internacionalização (POCI) with the reference project POCI-01-0145-FEDER-006941.

Author contribution statement

Conceptualization: G. Miranda, F. S. Silva and M. Gasik made the design of this study

Investigation:

- F. Bartolomeu and N. Alves took part in the fabrication by additive manufacturing of Ti6Al4V structures
- M.M. Costa and F. Melo-Fonseca fabricated the BAG-Ti6Al4V structures
- F. Melo-Fonseca and M. M. Costa made the additional experimental characterization

- R. Lima, A. Miranda and N. A. Silva made the biological studies;
- Miranda made the statistical analysis

Funding acquisition and Resources: G. Miranda, F. Bartolomeu; F. S. Silva; R. Lima and N. A. Silva (projects and individual grants)

Supervision: G. Miranda, N. A. Silva and F. S. Silva

Writing - original draft: F. Melo-Fonseca, M.M. Costa, M. Gasik, F. S. Silva and G. Miranda wrote the paper.

Writing - review & editing: F. Melo-Fonseca, G. Miranda and N.A. Silva did the review and editing.

References

[1] S.J.F. MD, 100 Questions & Answers About Hip Replacement, Jones, 2010.
[2] S. Affatato, Perspectives in Total Hip Arthroplasty - Advances in Biomaterials and Their Tribological Interactions, Woodhead P, 2014https://doi.org/10.1016/B978-1-78242-031-6.50016-7.
[3] S.D. Ulrich, T.M. Seyler, D. Bennett, R.E. Delanois, K.J. Saleh, I. Thongtrangan, M. Kuskowski, E.Y. Cheng, P.F. Sharkey, J. Parvizi, J.B. Stiehl, M.A. Mont, Total hip arthroplasties: what are the reasons for revision? Int. Orthop. 32 (2008) 597–604, https://doi.org/10.1007/s00264-007-0364-3.
[4] U. Holzwarth, G. Cotogno, Total hip arthroplasty - state of the art, Challenges and Prospects, 2012https://doi.org/10.2788/31286.
[5] G. Ryan, A. Pandit, D.P. Apatsidis, Fabrication methods of porous metals for use in orthopaedic applications, Biomaterials 27 (2006) 2651–2670, https://doi.org/10.1016/j.biomaterials.2005.12.002.
[6] D.F. Williams, in: D.F. Williams (Ed.), Definitions in Biomaterials, Elsevier, Amsterdam, 1987https://doi.org/10.1002/pol.1988.140260910 , (72 pp., J. Polym. Sci. Polym. Lett. Ed. 26 (1988) 414–414).
[7] E. Ingham, J. Fisher, The role of macrophages in osteolysis of total joint replacement, Biomaterials 26 (2005) 1271–1286, https://doi.org/10.1016/j.biomaterials.2004.04.035.
[8] G. Li, L. Wang, W. Pan, F. Yang, W. Jiang, X. Wu, X. Kong, K. Dai, Y. Hao, In vitro and in vivo study of additive manufactured porous Ti6Al4V scaffolds for repairing bone defects, Sci. Rep. 6 (2016) 1–11, https://doi.org/10.1038/srep34072.
[9] W. Wang, C.K. Poh, Titanium alloys in orthopaedics, Singapore, 2013.
[10] X.P. Tan, Y.J. Tan, C.S.L. Chow, S.B. Tor, W.Y. Yeong, Metallic powder-bed based 3D printing of cellular scaffolds for orthopaedic implants: a state-of-the-art review on manufacturing, topological design, mechanical properties and biocompatibility, Mater. Sci. Eng. C 76 (2017) 1328–1343, https://doi.org/10.1016/j.msec.2017.02.094.
[11] S. Zhao, S.J. Li, W.T. Hou, Y.L. Hao, R. Yang, L.E. Murr, Microstructure and mechanical properties of open cellular Ti–6Al–4V prototypes fabricated by electron beam melting for biomedical applications, Mater. Technol. 7857 (2016) 1–10, https://doi.org/10.1179/1753555715Y.0000000056.
[12] A. Kumar, S. Mandal, S. Barui, R. Vasireddi, U. Gbureck, M. Gelinsky, B. Basu, Low temperature additive manufacturing of three dimensional scaffolds for bone-tissue engineering applications: processing related challenges and property assessment, Mater. Sci. Eng. R. Rep. 103 (2016) 1–39, https://doi.org/10.1016/j.mser.2016.01.001.
[13] J.D. Bobyn, R.M. Pilliar, H.U. Cameron, G.C. Weatherly, The optimum pore size for the fixation of porous-surfaced metal implants by the ingrowth of bone, Clin. Orthop. Relat. Res. (1980) 263–270 http://www.ncbi.nlm.nih.gov/pubmed/7428231 (accessed April 21, 2017).
[14] D. Apostu, O. Lucaciu, C. Berce, D. Lucaciu, D. Cosma, Current methods of preventing aseptic loosening and improving osseointegration of titanium implants in cementless total hip arthroplasty: a review, J. Int. Med. Res. 0 (2017), 030006051773269. https://doi.org/10.1177/0300060517732697.
[15] T. Zhou, Y. Zhu, X. Li, X. Liu, K.W.K. Yeung, S. Wu, X. Wang, Z. Cui, X. Yang, P.K. Chu, Surface functionalization of biomaterials by radical polymerization, Prog. Mater. Sci. 83 (2016) 191–235, https://doi.org/10.1016/j.pmatsci.2016.04.005.
[16] X. Liu, M. Li, Y. Zhu, K.W.K. Yeung, P.K. Chu, S. Wu, The modulation of stem cell behaviors by functionalized nanoceramic coatings on Ti-based implants, Bioact. Mater. 1 (2016) 65–76, https://doi.org/10.1016/j.bioactmat.2016.09.001.
[17] Y. Zhang, X. Liu, Z. Li, S. Zhu, X. Yuan, Z. Cui, X. Yang, P.K. Chu, S. Wu, Nano Ag/ZnO-incorporated hydroxyapatite composite coatings: highly effective infection prevention and excellent osteointegration, ACS Appl. Mater. Interfaces 10 (2018) 1266–1277, https://doi.org/10.1021/acsami.7b17351.
[18] M. Li, X. Liu, Z. Xu, K.W.K. Yeung, S. Wu, Dopamine modified organic-inorganic hybrid coating for antimicrobial and osteogenesis, ACS Appl. Mater. Interfaces 8 (2016) 33972–33981, https://doi.org/10.1021/acsami.6b09457.
[19] J. Li, L. Tan, X. Liu, Z. Cui, X. Yang, K.W.K. Yeung, P.K. Chu, S. Wu, Balancing bacteria-osteoblast competition through selective physical puncture and biofunctionalization of ZnO/polydopamine/arginine-glycine-aspartic acid-cysteine nanorods, ACS Nano 11 (2017) 11250–11263, https://doi.org/10.1021/acsnano.7b05620.
[20] K. Zhang, Y. Zhu, X. Liu, Z. Cui, Y. Xianjin, K.W.K. Yeung, H. Pan, S. Wu, Sr/ZnO doped titania nanotube array: an effective surface system with excellent osteoinductivity and self-antibacterial activity, Mater. Des. 130 (2017) 403–412, https://doi.org/10.1016/j.matdes.2017.05.085.
[21] J. Vaithilingam, S. Kilsby, R.D. Goodridge, S.D.R. Christie, S. Edmondson, R.J.M. Hague, Functionalisation of Ti6Al4V components fabricated using selective laser melting with a bioactive compound, Mater. Sci. Eng. C 46 (2015) 52–61, https://doi.org/10.1016/j.msec.2014.10.015.
[22] S.L. Sing, S. Wang, S. Agarwala, F.E. Wiria, T. Mai, H. Ha, W.Y. Yeong, Fabrication of titanium based biphasic scaffold using selective laser melting and collagen immersion, Int. J. Bioprinting 3 (2017) 1–7, https://doi.org/10.18063/IJB.2017.01.007.
[23] M. Santin, G. Philips, Biomimetic, Bioresponsive, and Bioactive Materials - An Introduction to Integrating Materials With Tissues, Wiley, John Wiley & Sons, 2012.
[24] O. Guillon, S. Cao, J. Chang, L. Wondraczek, A.R. Boccaccini, Effect of uniaxial load on the sintering behaviour of 45S5 Bioglass powder compacts, J. Eur. Ceram. Soc. 31 (2011) 999–1007, https://doi.org/10.1016/j.jeurceramsoc.2010.12.031.
[25] O. Bretcanu, X. Chatzistavrou, K. Paraskevopoulos, R. Conradt, I. Thompson, A.R. Boccaccini, Sintering and crystallisation of 45S5 Bioglass® powder, J. Eur. Ceram. Soc. 29 (2009) 3299–3306, https://doi.org/10.1016/j.jeurceramsoc.2009.06.035.
[26] A.A. El-Rashidy, J.A. Roether, L. Harhaus, U. Kneser, A.R. Boccaccini, Regenerating bone with bioactive glass scaffolds: a review of in vivo studies in bone defect models, Acta Biomater. 62 (2017) 1–28, https://doi.org/10.1016/j.actbio.2017.08.030.
[27] P. Ducheyne, Bioactive ceramics: the effect of surface reactivity on bone formation and bone cell function, Biomaterials 20 (1999) 2287–2303, https://doi.org/10.1016/S0142-9612(99)00181-7.
[28] W. Leenakul, T. Tunkasiri, N. Tongsiri, K. Pengpat, J. Ruangsuriya, Effect of sintering temperature variations on fabrication of 45S5 bioactive glass-ceramics using rice husk as a source for silica, Mater. Sci. Eng. C 61 (2016) 695–704, https://doi.org/10.1016/j.msec.2015.12.029.
[29] S. Grasso, R.K. Chinnam, H. Porwal, A.R. Boccaccini, M.J. Reece, Low temperature spark plasma sintering of 45S5 Bioglass®, J. Non-Cryst. Solids 362 (2013) 25–29, https://doi.org/10.1016/j.jnoncrysol.2012.11.009.
[30] M.N. Rahaman, D.E. Day, B.S. Bal, Q. Fu, S.B. Jung, L.F. Bonewald, A.P. Tomsia, Bioactive glass in tissue engineering, Acta Biomater. 7 (2011) 2355–2373, https://doi.org/10.1016/j.actbio.2011.03.016.
[31] D. Bellucci, V. Cannillo, A. Sola, An overview of the effects of thermal processing on bioactive glasses, Sci. Sinter. 42 (2010) 307–320, https://doi.org/10.2298/SOS1003307B.
[32] N. Drnovšek, S. Novak, U. Dragin, M. Čeh, M. Gorenšek, M. Gradišar, Bioactive glass enhances bone ingrowth into the porous titanium coating on orthopaedic implants, Int. Orthop. 36 (2012) 1739–1745, https://doi.org/10.1007/s00264-012-1520-y.
[33] D.F. Williams, On the mechanisms of biocompatibility, Biomaterials 29 (2008) 2941–2953, https://doi.org/10.1016/j.biomaterials.2008.04.023.
[34] G. Miranda, S. Faria, F. Bartolomeu, E. Pinto, S. Madeira, A. Mateus, P. Carreira, Predictive models for physical and mechanical properties of 316L stainless steel produced by selective laser melting, Mater. Sci. Eng. A 657 (2016) 43–56, https://doi.org/10.1016/j.msea.2016.01.028.
[35] M.U. Jurczyk, K. Jurczyk, A. Miklaszewski, M. Jurczyk, Nanostructured titanium-45S5 Bioglass scaffold composites for medical applications, Mater. Des. 32 (2011) 4882–4889, https://doi.org/10.1016/j.matdes.2011.06.005.
[36] R.M. German, Powder Metallurgy & Particulate Materials Processing, Metal Powd, Princeton, 2005.
[37] G.S. Upadhyaya, Powder Metallurgy Technology, Cambridge International Science Publishing, 1997https://doi.org/10.1073/pnas.0703993104.
[38] G. Miranda, Development of Aluminum Based Composites by Pressure-assisted Sintering, Universidade do Minho, 2015.
[39] A. Popovich, V. Sufiiarov, Metal powder additive manufacturing, New Trends 3D Print, InTech, 2016https://doi.org/10.5772/63337.
[40] R. Singh, V. Bhavar, P. Kattire, S. Thakare, S. Patil, R.K.P. Singh, A review on functionally gradient materials (FGMs) and their applications, IOP Conf. Ser. Mater. Sci. Eng, vol. 229, 2017 https://doi.org/10.1088/1757-899X/229/1/012021.
[41] B. Thavornyutikarn, N. Chantarapanich, K. Sitthiseripratip, G.A. Thouas, Q. Chen, Bone Tissue Engineering Scaffolding: Computer-aided Scaffolding Techniques, 2014https://doi.org/10.1007/s40204-014-0026-7.
[42] O. Al-Ketan, R. Rowshan, R.K. Abu Al-Rub, Topology-mechanical property relationship of 3D printed strut, skeletal, and sheet based periodic metallic cellular materials, Addit. Manuf. 19 (2018) 167–183, https://doi.org/10.1016/j.addma.2017.12.006.
[43] L.-C. Zhang, H. Attar, Selective laser melting of titanium alloys and titanium matrix composites for biomedical applications: a review, Adv. Eng. Mater. 18 (2016) 463–475, https://doi.org/10.1002/adem.201500419.
[44] A.M. Khorasani, I. Gibson, M. Goldberg, G. Littlefair, A survey on mechanisms and critical parameters on solidification of selective laser melting during fabrication of Ti-6Al-4V prosthetic acetabular cup, Mater. Des. 103 (2016) 348–355, https://doi.org/10.1016/j.matdes.2016.04.074.
[45] V. Weißmann, R. Bader, H. Hansmann, N. Laufer, Influence of the structural orientation on the mechanical properties of selective laser melted, Mater. Des. 95 (2016) 188–197, https://doi.org/10.1016/j.matdes.2016.01.095.
[46] S. Bose, D. Ke, H. Sahasrabudhe, A. Bandyopadhyay, Progress in materials science additive manufacturing of biomaterials, Prog. Mater. Sci. 93 (2018) 45–111, https://doi.org/10.1016/j.pmatsci.2017.08.003.
[47] Z.S. Bagheri, D. Melancon, L. Liu, R.B. Johnston, D. Pasini, Compensation strategy to reduce geometry and mechanics mismatches in porous biomaterials built with Selective Laser Melting, J. Mech. Behav. Biomed. Mater. 70 (2017) 17–27, https://doi.org/10.1016/j.jmbbm.2016.04.041.
[48] B. Van Hooreweder, Y. Apers, K. Lietaert, J.-P. Kruth, Improving the fatigue performance of porous metallic biomaterials produced by Selective Laser Melting, Acta Biomater. 47 (2017) 193–202, https://doi.org/10.1016/j.actbio.2016.10.005.
[49] J. Vaithilingam, E. Prina, R.D. Goodridge, R.J.M. Hague, S. Edmondson, F.R.A.J. Rose, S.D.R. Christie, Surface chemistry of Ti6Al4V components fabricated using selective laser melting for biomedical applications, Mater. Sci. Eng. C 67 (2016) 294–303, https://doi.org/10.1016/j.msec.2016.05.054.

[50] W. Duan, Y. Yin, J. Zhou, Temperature Field Simulations During Selective Laser Melting Process Based on Fully Threaded Tree, 14, China Foundry, 2017 405–411.
[51] P. Li, Q. Yang, F. Zhang, T. Kokubo, The effect of residual glassy phase in a bioactive glass-ceramic on the formation of its surface apatite layer in vitro, J. Mater. Sci. Mater. Med. 3 (1992) 452–456, https://doi.org/10.1007/BF00701242.
[52] D. Bellucci, A. Sola, V. Cannillo, Low temperature sintering of innovative bioactive glasses, J. Am. Ceram. Soc. 95 (2012) 1313–1319, https://doi.org/10.1111/j.1551-2916.2012.05100.x.
[53] Straumann, Straumann SLA, Sci. Evid, first ed., 2011 1–36.
[54] P. Ming, S. Shao, J. Qiu, J. Yang, Y. Yu, J. Chen, W. Zhu, C. Tang, Superiority of calcium-containing nanowires modified titanium surface compared with SLA titanium surface in biological behavior of osteoblasts: a pilot study, Appl. Surf. Sci. 416 (2017) 790–797, https://doi.org/10.1016/j.apsusc.2017.04.152.
[55] F. Bartolomeu, S. Faria, O. Carvalho, E. Pinto, N. Alves, F.S. Silva, G. Miranda, Predictive models for physical and mechanical properties of Ti6Al4V produced by Selective Laser Melting, Mater. Sci. Eng. A 663 (2016) 181–192, https://doi.org/10.1016/j.msea.2016.03.113.
[56] F. Bartolomeu, M. Sampaio, O. Carvalho, E. Pinto, N. Alves, J.R. Gomes, F.S. Silva, G. Miranda, Tribological behavior of Ti6Al4V cellular structures produced by Selective Laser Melting, J. Mech. Behav. Biomed. Mater. 69 (2017) 128–134, https://doi.org/10.1016/j.jmbbm.2017.01.004.
[57] ISO 4287:1997, Geometrical product specifications (GPS) — surface texture: profile method — terms, definitions and surface texture parameters, Int. Organ. Stand. (1997)https://www.iso.org/standard/10132.html.
[58] N.A. Silva, A.J. Salgado, R.A. Sousa, J.T. Oliveira, A.J. Pedro, H. Leite-Almeida, R. Cerqueira, A. Almeida, F. Mastronardi, J.F. Mano, N.M. Neves, N. Sousa, R.L. Reis, Development and characterization of a novel hybrid tissue engineering–based scaffold for spinal cord injury repair, Tissue Eng. A 16 (2010) 45–54, https://doi.org/10.1089/ten.tea.2008.0559.
[59] S. Ribeiro-Samy, N.A. Silva, V.M. Correlo, J.S. Fraga, L. Pinto, A. Teixeira-Castro, H. Leite-Almeida, A. Almeida, J.M. Gimble, N. Sousa, A.J. Salgado, R.L. Reis, Development and characterization of a PHBHV-based 3D scaffold for a tissue engineering and cell-therapy combinatorial approach for spinal cord injury regeneration, Macromol. Biosci. 13 (2013) 1576–1592, https://doi.org/10.1002/mabi.201300178.
[60] N. Teraphongphom, P. Chhour, J.R. Eisenbrey, P.C. Naha, W.R.T. Witschey, B. Opasanont, L. Jablonowski, D.P. Cormode, M.A. Wheatley, Nanoparticle loaded polymeric microbubbles as contrast agents for multimodal imaging, Langmuir 31 (2015) 11858–11867, https://doi.org/10.1021/acs.langmuir.5b03473.
[61] P. Chhour, N. Gallo, R. Cheheltani, D. Williams, A. Al-Zaki, T. Paik, J.L. Nichol, Z. Tian, P.C. Naha, W.R. Witschey, H.R. Allcock, C.B. Murray, A. Tsourkas, D.P. Cormode, Nanodisco balls: control over surface versus core loading of diagnostically active nanocrystals into polymer nanoparticles, ACS Nano 8 (2014) 9143–9153, https://doi.org/10.1021/nn502730q.
[62] A. Canha-Gouveia, A. Rita Costa-Pinto, A.M. Martins, N.A. Silva, S. Faria, R.A. Sousa, A.J. Salgado, N. Sousa, R.L. Reis, N.M. Neves, Hierarchical scaffolds enhance osteogenic differentiation of human Wharton's jelly derived stem cells, Biofabrication 7 (2015) 35009, https://doi.org/10.1088/1758-5090/7/3/035009.
[63] R. Silva, H. Ferreira, A.C. Carvalho, A.C. Gomes, A. Cavaco-Paulo, Protein microspheres as suitable devices for piroxicam release, Colloids Surf. B: Biointerfaces 92 (2012) 277–285, https://doi.org/10.1016/j.colsurfb.2011.11.050.
[64] S. Zhang, Q. Wei, L. Cheng, S. Li, Y. Shi, Effects of scan line spacing on pore characteristics and mechanical properties of porous Ti6Al4V implants fabricated by selective laser melting, Mater. Des. 63 (2014) 185–193, https://doi.org/10.1016/j.matdes.2014.05.021.
[65] J. Christian, The Theory of Transformations in Metals and Alloys, first ed. Pergamon, 2002.
[66] A.R. Boccaccini, Q. Chen, L. Lefebvre, L. Gremillard, J. Chevalier, Sintering, crystallisation and biodegradation behaviour of Bioglass®-derived glass–ceramics, Faraday Discuss. 136 (2007) 27, https://doi.org/10.1039/b616539g.
[67] L. Lefebvre, J. Chevalier, L. Gremillard, R. Zenati, G. Thollet, D. Bernache-Assolant, A. Govin, Structural transformations of bioactive glass 45S5 with thermal treatments, Acta Mater. 55 (2007) 3305–3313, https://doi.org/10.1016/j.actamat.2007.01.029.
[68] L. Ponsonnet, K. Reybier, N. Jaffrezic, V. Comte, C. Lagneau, M. Lissac, C. Martelet, Relationship between surface properties (roughness, wettability) of titanium and titanium alloys and cell behaviour, Mater. Sci. Eng. C 23 (2003) 551–560, https://doi.org/10.1016/S0928-4931(03)00033-X.
[69] N.J. Hallab, K.J. Bundy, K. O'Connor, R.L. Moses, J.J. Jacobs, Evaluation of metallic and polymeric biomaterial surface energy and surface roughness characteristics for directed cell adhesion, Tissue Eng. 7 (2001) 55–71, https://doi.org/10.1089/107632700300003297.
[70] L. Ponsonnet, V. Comte, A. Othmane, C. Lagneau, M. Charbonnier, M. Lissac, N. Jaffrezic, Effect of surface topography and chemistry on adhesion, orientation and growth of fibroblasts on nickel-titanium substrates, Mater. Sci. Eng. C 21 (2002) 157–165, https://doi.org/10.1016/S0928-4931(02)00097-8.
[71] C.-J. Chen, S.-J. Ding, C.-C. Chen, Effects of surface conditions of titanium dental implants on bacterial adhesion, Photomed. Laser Surg. 34 (2016), pho.2016.4103. https://doi.org/10.1089/pho.2016.4103.
[72] M. Taborelli, M. Jobin, P. François, P. Vaudaux, M. Tonetti, S. Szmukler-Moncler, J. Simpson, P. Descouts, Influence of surface treatments developed for oral implants on the physical and biological properties of titanium. Surface characterization, Clin. Implant Dent. Relat. Res. 8 (1997) 208–216.
[73] J. Vaithilingam, S. Kilsby, R.D. Goodridge, S.D.R. Christie, S. Edmondson, R.J.M. Hague, Functionalisation of Ti6Al4V components fabricated using selective laser melting with a bioactive compound, Mater. Sci. Eng. C 46 (2015) 52–61, https://doi.org/10.1016/j.msec.2014.10.015.
[74] E.A. Vogler, Structure and reactivity of water at biomaterial surfaces, Adv. Colloid Interf. Sci. 74 (1998) 69–117, https://doi.org/10.1016/S0001-8686(97)00040-7.
[75] L. Le Guéhennec, A. Soueidan, P. Layrolle, Y. Amouriq, Surface treatments of titanium dental implants for rapid osseointegration, Dent. Mater. 23 (2007) 844–854, https://doi.org/10.1016/J.DENTAL.2006.06.025.
[76] G. Zhao, Z. Schwartz, M. Wieland, F. Rupp, J. Geis-Gerstorfer, D.L. Cochran, B.D. Boyan, High surface energy enhances cell response to titanium substrate microstructure, J. Biomed. Mater. Res. A 74 (2005) 49–58, https://doi.org/10.1002/jbm.a.30320.
[77] R.A. Gittens, T. McLachlan, Y. Cai, S. Berner, R. Tannenbaum, Z. Schwartz, K.H. Sandhage, B.D. Boyan, The effects of combined micron-/submicron-scale surface roughness and nanoscale features on cell proliferation and differentiation, Biomaterials 32 (2011) 3395–3403, https://doi.org/10.1016/j.biomaterials.2011.01.029.The.
[78] W. Li, P. Nooeaid, J.A. Roether, D.W. Schubert, A.R. Boccaccini, Preparation and characterization of vancomycin releasing PHBV coated 45S5 Bioglass®-based glass-ceramic scaffolds for bone tissue engineering, J. Eur. Ceram. Soc. 34 (2014) 505–514, https://doi.org/10.1016/j.jeurceramsoc.2013.08.032.
[79] W. Li, N. Garmendia, U. Pérez de Larraya, Y. Ding, R. Detsch, A. Grünewald, J.A. Roether, D.W. Schubert, A.R. Boccaccini, 45S5 bioactive glass-based scaffolds coated with cellulose nanowhiskers for bone tissue engineering, RSC Adv. 4 (2014) 56156–56164, https://doi.org/10.1039/C4RA07740G.
[80] R.N. Wenzel, Resistance of solid surfaces to wetting by water, Ind. Eng. Chem. 28 (1936) 988–994, https://doi.org/10.1021/ie50320a024.
[81] A.B.D. Cassie, S. Baxter, Wettability of porous surfaces, Trans. Faraday Soc. 40 (1944) 546–551, https://doi.org/10.1039/TF9444000546.
[82] S.P. Rodrigues, C.F.A. Alves, A. Cavaleiro, S. Carvalho, Water and oil wettability of anodized 6016 aluminum alloy surface, Appl. Surf. Sci. 422 (2017) 430–442, https://doi.org/10.1016/j.apsusc.2017.05.204.
[83] D. Yamamoto, Osteoconductivity of superhydrophilic anodized TiO_2 coatings on Ti treated with hydrothermal processes, J. Biomater. Nanobiotechnol. 04 (2013) 45–52, https://doi.org/10.4236/jbnb.2013.41007.
[84] M. Zuldesmi, K. Kuroda, M. Okido, Hydrothermal treatment of titanium alloys for enhancement of osteoconductivity, Mater. Sci. Eng. C 49 (2015) 430–435.
[85] J.I. Rosales-Leal, M.A. Rodríguez-Valverde, G. Mazzaglia, P.J. Ramón-Torregrosa, L. Díaz-Rodríguez, O. García-Martínez, M. Vallecillo-Capilla, C. Ruiz, M.A. Cabrerizo-Vílchez, Effect of roughness, wettability and morphology of engineered titanium surfaces on osteoblast-like cell adhesion, Colloids Surf. A Physicochem. Eng. Asp. 365 (2010) 222–229, https://doi.org/10.1016/j.colsurfa.2009.12.017.
[86] R.A. Gittens, L. Scheideler, F. Rupp, S.L. Hyzy, J. Geis-Gerstorfer, Z. Schwartz, B.D. Boyan, A review on the wettability of dental implant surfaces ii: biological and clinical aspects, Acta Biomater. 10 (2014) 2907–2918, https://doi.org/10.1109/TMI.2012.2196707.Separate.
[87] M. Wang, Y. Wu, S. Lu, T. Chen, Y. Zhao, H. Chen, Z. Tang, Fabrication and characterization of selective laser melting printed Ti–6Al–4V alloys subjected to heat treatment for customized implants design, Prog. Nat. Sci. Mater. Int. 26 (2016) 671–677, https://doi.org/10.1016/j.pnsc.2016.12.006.
[88] W. Busa, R. Nuccitelli, Metabolic regulation via intracellular pH, Am. J. Phys. 246 (1984) 409–438http://ajpregu.physiology.org/content/246/4/R409.short.
[89] J. Lu, M. Descamps, J. Dejou, G. Koubi, P. Hardouin, J. Lemaitre, J.P. Proust, The biodegradation mechanism of calcium phosphate biomaterials in bone, J. Biomed. Mater. Res. 63 (2002) 408–412, https://doi.org/10.1002/jbm.10259.
[90] L.-E. Monfoulet, P. Becquart, D. Marchat, K. Vandamme, M. Bourguignon, E. Pacard, V. Viateau, H. Petite, D. Logeart-Avramoglou, The pH in the microenvironment of human mesenchymal stem cells is a critical factor for optimal osteogenesis in tissue-engineered constructs, Tissue Eng. A 20 (2014) 1827–1840, https://doi.org/10.1089/ten.tea.2013.0500.
[91] I.A. Silver, J. Deas, M. Erecińska, Interactions of bioactive glasses with osteoblasts in vitro: effects of 45S5 Bioglass(®), and 58S and 77S bioactive glasses on metabolism, intracellular ion concentrations and cell viability, Biomaterials 22 (2001) 175–185, https://doi.org/10.1016/S0142-9612(00)00173-3.
[92] I. Allan, H. Newman, M. Wilson, Antibacterial activity of particulate Bioglass®against supra- and subgingival bacteria, Biomaterials 22 (2001) 1683–1687, https://doi.org/10.1016/S0142-9612(00)00330-6.
[93] J. Smachson, Basic requirements for calcification, Nature 221 (1969) 1247–1248, https://doi.org/10.1038/2211247a0.
[94] D.A. Bushinsky, Metabolic alkalosis decreases bone calcium efflux by suppressing osteoclasts and stimulating osteoblasts, Am. J. Physiol. Physiol. 271 (1996) F216–F222, https://doi.org/10.1152/ajprenal.1996.271.1.F216.
[95] W. Moody, Effects of intracellular H+ on the electrical properties of excitable cells, Annu. Rev. Neurosci. 7 (1984) 257–278, https://doi.org/10.1146/annurev.ne.07.030184.001353.